ASCE

Simulating Cyclic Local Buckling–Induced Softening in Steel Beam-Columns Using a Nonlocal Material Model in Displacement-Based Fiber Elements

Subodh Kolwankar, S.M.ASCE[1]; Amit Kanvinde, M.ASCE[2]; Maha Kenawy, S.M.ASCE[3]; Dimitrios Lignos, M.ASCE[4]; and Sashi Kunnath, F.ASCE[5]

Abstract: Steel beam-columns subjected to cyclic loading (such as during earthquakes) may exhibit local buckling, which results in effective cross-sectional softening and localization of deformation. These phenomena are critical from the standpoint of performance and collapse assessment. Fiber-based elements are attractive for simulating beam-column response because they capture P-M interactions and the spread of plasticity and can be generalized to different cross sections from material-level calibrations. However, conventional fiber models typically employ softening constitutive material laws to represent local buckling. Without a regularizing length scale, this results in a nonelliptic boundary-value problem, leading to severe mesh dependence. A two-dimensional nonlocal fiber-based beam-column model is presented to address this issue for steel wide-flange sections subject to combinations of axial and cyclic lateral loads. The methodology includes the following elements: (1) a constitutive material model that is able to represent inelastic cyclic local buckling, (2) a nonlocal strain formulation that incorporates a physically based length scale, and (3) suggested practices for input selection and parameter calibration. Forty-two continuum finite-element models (encompassing a range of parameters including cross section, axial load ratio, moment gradient, and loading history) are constructed to inform as well as validate the presented methodology. The methodology simulates various aspects (load-deformation response, localized deformation, and column axial shortening) with accuracy and without mesh dependence. This is in contrast to conventional fiber models that exhibit severe mesh dependence. Limitations are discussed. **DOI: 10.1061/(ASCE)ST.1943-541X.0002457.**

Author keywords: Fiber models; Localization; Nonlocal formulations; Frame elements; Deterioration; Steel beam-columns; Local buckling.

Introduction

Steel moment-resisting frames (SMRFs) designed in seismic regions rely on the cyclic inelastic response of members to dissipate energy and accommodate deformations [e.g., AISC 341 (AISC 2016)]. Accurate simulation of the cyclic hysteretic response of beams and columns is critical for the seismic performance assessment of these frames from the onset of damage through collapse. Referring to Fig. 1(a), the cyclic hysteretic response of these members [shown for a test conducted previously by Elkady and Lignos (2018a)] exhibits characteristics including yielding, cyclic hardening, cycle-to-cycle flexural strength, and stiffness deterioration, followed by in-cycle strength loss after the attainment of peak strength. This response arises from interactions between steel material yielding and geometric instabilities associated with cyclic local buckling or lateral-torsional buckling. The postpeak response—specifically the negative slope, is a dominant parameter influencing the collapse of SMRF systems (Ibarra and Krawinkler 2005; Lignos et al. 2011, 2013). As a result, accurate representation of the postpeak response is consequential, especially because guidelines for building performance assessment [FEMA P695 (FEMA 2009); PEER 2010; ASCE 7 (ASCE 2017); LATBSDC 2017] rely heavily on accuracy in dynamic collapse simulations. The physical mechanisms responsible for the hysteretic behavior shown in Fig. 1(a) (i.e., cyclic local buckling, multiaxial plasticity, lateral-torsional instability) with the possible exception of fracture, can be conveniently simulated through continuum finite-element (CFE) simulations that incorporate cyclic plasticity, large deformations, and appropriate mesh refinement, as demonstrated by Elkady and Lignos (2015, 2018b). However, such simulations are seldom used for building performance assessment due to their high computational cost, especially when large suites of nonlinear response history simulations are mandated to characterize the earthquake-induced collapse risk of frame structures (e.g., as per FEMA P695). Frame element–based simulations with concentrated plastic hinges (Dides and de la Llera 2005; Ibarra et al. 2005) and distributed plasticity are the currently preferred methods of simulation. Each of these methods has its limitations (Kolwankar et al. 2018). Plastic hinge models are not facile with respect to simulation of P-M interaction, cannot simulate yielding in arbitrary locations, and require component tests for calibration (e.g., Lignos and Krawinkler 2013), so they are

[1]Graduate Research Assistant, Dept. of Civil and Environmental Engineering, Univ. of California, Davis, CA 95616.

[2]Professor, Dept. of Civil and Environmental Engineering, Univ. of California, Davis, CA 95616 (corresponding author). Email: kanvinde@ucdavis.edu

[3]Graduate Research Assistant, Dept. of Civil and Environmental Engineering, Univ. of California, Davis, CA 95616. ORCID: https://orcid.org/0000-0002-9722-091X

[4]Associate Professor, Dept. of Architecture, Civil and Environmental Engineering, Ecole Polytechnique Fédérale de Lausanne, Lausanne 1015 CH, Switzerland. ORCID: https://orcid.org/0000-0003-0682-4660

[5]Professor, Dept. of Civil and Environmental Engineering, Univ. of California, Davis, CA 95616.

Note. This manuscript was submitted on July 26, 2018; approved on April 25, 2019; published online on October 29, 2019. Discussion period open until March 29, 2020; separate discussions must be submitted for individual papers. This paper is part of the ***Journal of Structural Engineering***, © ASCE, ISSN 0733-9445.

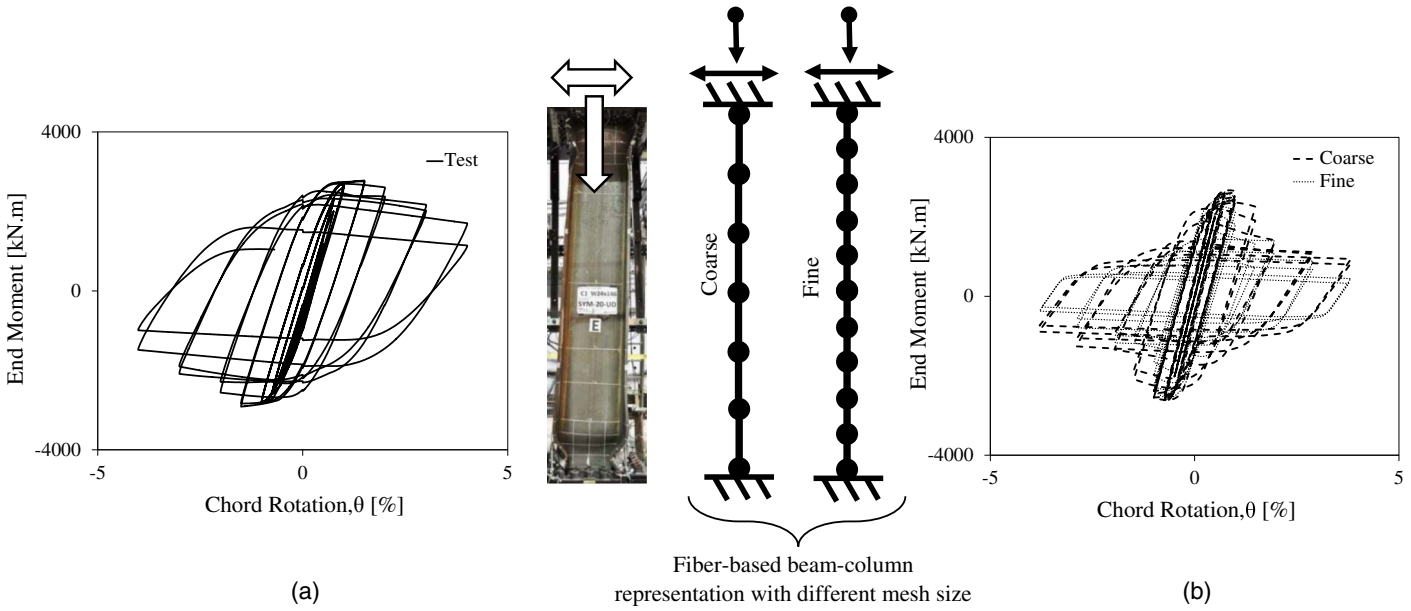

Fig. 1. (a) Moment versus rotation curve for rolled W-section W24 × 146 at 0.2*Py*; and (b) simulation results using two different mesh sizes with fiber-based elements and softening constitutive response.

challenging to generalize. Distributed plasticity elements (whose most popular variant is fiber elements) (Spacone and Filippou 1996) overcome some of these limitations by utilizing fiber- or material-level calibrations that may be generalized to different cross sections, while also simulating P-M interaction and spread of plasticity. However, these suffer from severe mesh dependence when material constitutive softening is used to represent postpeak behavior. This type of mesh dependence (or nonobjectivity) is a well-studied phenomenon in both continuum (Bazant and Jirasek 2002) and fiber-element simulations (Coleman and Spacone 2001). From a theoretical point of view, this occurs because as the mesh is refined, the numerical solution converges to the analytical solution, which is singular if softening constitutive models are used without a concomitant length scale. In practical terms, this means that the mesh size (or Gauss-point spacing) acts as an arbitrary length scale over which deformations localize, while the neighboring regions unload elastically. Fig. 1(b) illustrates this type of mesh dependence in the context of frame members simulated with fiber elements. Given the sensitivity of collapse to postpeak response (including negative slope and degradation), such mesh dependence is problematic for the reliable performance and collapse assessment of structures. Research over the last four decades has sought to address the problem of mesh dependence in continuum models; the main outcome is that introducing a physically based length scale regularizes the analytical solution, thereby preventing the mesh size from acting as an arbitrary, surrogate length scale (Wu and Wang 2008, 2010). This length scale may be introduced by fixing the plastic hinge length (e.g., Kasai et al. 2016; Suzuki and Lignos 2018) by synchronizing the mesh size with the softening slope (informed by parameters such as fracture energy) (Coleman and Spacone 2001) or by enriching the strain or curvature fields through "nonlocal" formulations that distribute the strain over a region defined by a characteristic length, rather than the mesh size. In contrast to conventional "local" constitutive models, which assume that constitutive response (e.g., stress) at any location depends only on the strain at that location, nonlocal models are based on the assumption that the stress at any "host" location may be related to "receiver" locations in the vicinity of the host. From a mathematical standpoint, this facilitates the insertion of a length scale to regularize an otherwise ill-posed problem (Bazant and Jirasek 2002). From a physical standpoint, this allows for the reintroduction of mechanisms underlying three-dimensional (3D) responses (e.g., local buckling) that cannot be directly simulated within the numerical construct of fiber elements [i.e., one-dimensional (1D) representation of buckling-induced softening]. In doing so, nonlocal formulations mitigate the mesh dependence of both the global load-deformation response as well as the local strain distributions. Although fairly common for continuum modeling, they are less established for frame elements, having been the subject of study for the last decade (Valipour and Foster 2009; Salehi and Sideris 2017, 2018; Sideris and Salehi 2016; Zhang and Khandelwal 2016; Khaloo and Tariverdilo 2002, 2003). These studies have focused on localization due to concrete crushing, wherein softening (as observed at the continuum scale) may be attributed to material damage. Kolwankar et al. (2017) developed a nonlocal formulation to simulate geometric nonlinearity–induced softening (due to tension necking and compression buckling) in steel bars. Subsequently, Kolwankar et al. (2018) incorporated this formulation into a two-dimensional (2D) beam-column fiber element to represent local buckling–induced softening in wide-flanged sections subjected to monotonically applied axial and flexural loads. In light of the introductory discussion on SMRFs, the latter studies are promising because the dominant strength degradation and loss mechanisms in steel members are controlled by geometric nonlinearities such as local buckling. However, these do not address cyclic loading and cyclic deterioration in strength and stiffness [as noted in Fig. 1(a)], which is necessary for nonlinear response history simulations conducted in support of performance-based earthquake engineering. Motivated by this, this paper extends this formulation to a 2D beam-column element, which is able to simulate cyclic response including local buckling–induced softening in a mesh-independent manner. The paper leverages some previously developed aspects of nonlocal formulations (Kolwankar et al. 2017, 2018) for geometric nonlinearity (general functional forms, observations about localization length, and algorithmic implementation) while introducing new aspects

that specifically address cyclic loading applications. These include a cyclic constitutive model and attendant modifications to the nonlocal strain formulation to accommodate this cyclic model.

The paper begins by providing an overview of the physical response that the formulation seeks to simulate, i.e., the cyclic inelastic response of beam-columns subjected to flexural and axial loads, whose postpeak response is controlled by local buckling. To this end, the paper relies on previously conducted experiments (Elkady and Lignos 2018a) as well as CFE simulations conducted as part of this study; these inform aspects of the formulation, in addition to serving as a validation testbed for the developed approach. The CFE simulations may be considered virtual experiments that supplement the physical tests while providing insights into localized behavior (e.g., the evolution of localization length and fiber-level constitutive response) that cannot be obtained conveniently from the physical tests. This is followed by a discussion of the nonlocal formulation itself, which is subsequently applied to the CFE simulations and experiments to examine its efficacy in reproducing response (both global and local) while mitigating mesh dependency. The paper concludes by providing guidelines for application of the formulation while outlining its limitations and areas for future work.

Physical Response of Cyclically Loaded Wide-Flange Beam-Columns

Owing to the increased emphasis on simulation-based collapse assessment, recent experimental and computational studies have examined the inelastic cyclic response of wide-flange beam-columns. This section outlines findings from these studies as they pertain to the formulation presented in this paper. These observations are presented in an aggregated sense [based on studies by Elkady and Lignos (2018a), Newell and Uang (2008), and Suzuki and Lignos (2015)] to focus on mechanisms that control characteristics of load-deformation and localization response. The mechanisms and their progression presented here reflects the behavior of "moderately ductile" and "highly ductile" sections [i.e., sections with low width–thickness ratios defined as per AISC 341 (AISC 2016)] that reflect current seismic construction practice. Fig. 2 schematically illustrates the evolution of the load-deformation curve of a cantilever column (braced against lateral-torsional buckling) and the accompanying physical mechanisms responsible for each phase in this evolution.

The response is linear elastic until yielding initiates in the flanges. Subsequent to yielding, the lateral load and end moment continue to increase owing to strain hardening and increased plastification of the cross section. Since the sections are compact, no form of instability (e.g., local buckling) is observed before attainment of full plastic moment (Point 2). After this, the load deformation response exhibits a plateau, which continues until either the load is reversed or some form of geometric instability is encountered.

Local buckling in the flanges or web (Point 3) results in a negative stiffness and loss in load-carrying capacity. As the amplitude of the buckle increases, the buckling propagates into the web or flanges.

Reversed loading results in a similar sequence of events in the opposite direction, accompanied by straightening of the buckled flange, and buckling of the opposite flange depending on the presence and magnitude of the applied axial load ratio—Point 4.

Reloading in the forward direction (Point 5) results in a response similar to Points 1–3 with two exceptions. First, significant strength degradation is observed with respect to the preceding cycle; this is attributed to residual strains and buckling deformations from the previous cycle. Second, axial shortening is observed because the buckling strains on the opposite flange cannot be fully recovered upon loading in the forward direction (Elkady and Lignos 2018a).

The above phases may continue until accumulated strains induce fracture, or other forms of instability (e.g., lateral torsional buckling) or sideways collapse occurs. The global load-deformation

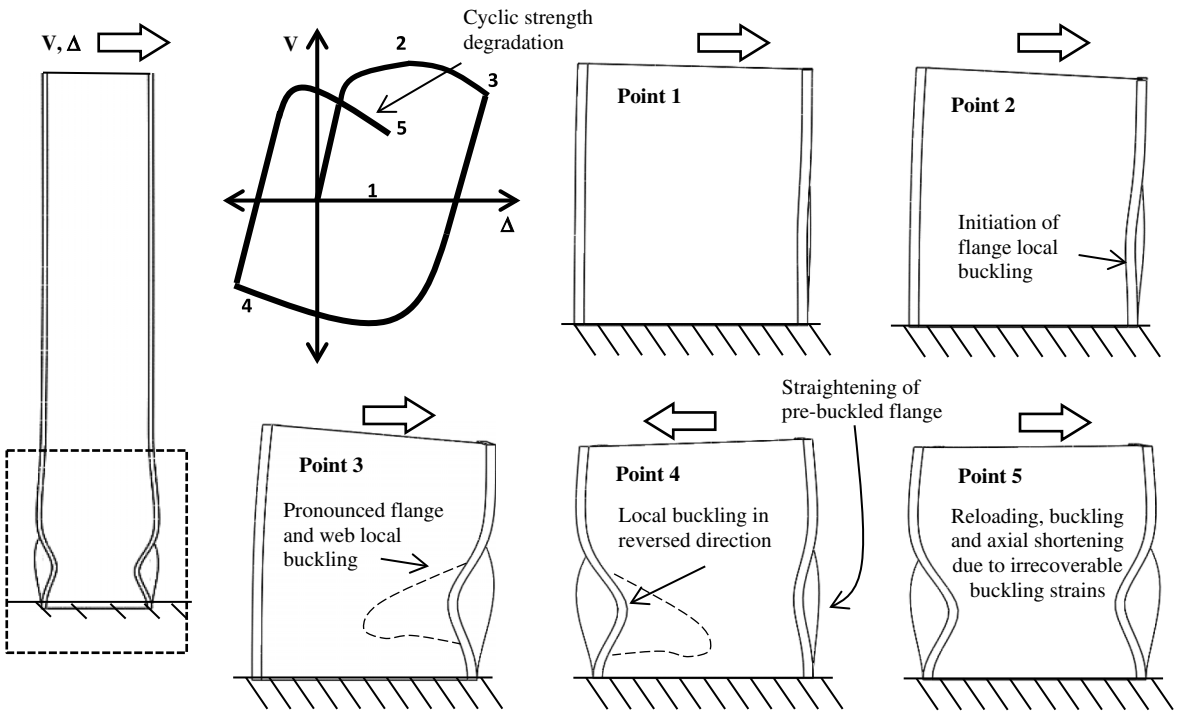

Fig. 2. Progression of load-deformation response and associated response modes in W-sections subjected to reversed cyclic loading.

response detailed above is the result of cyclic response of the regions of the cross section (mostly the flange and some portion of the web) participating in the progression of damage due to local buckling. This local response is detailed in subsequent sections, since it is a direct input to the nonlocal formulation. This section summarizes only its main aspects:

As portions of the flange buckle, they lose load-carrying capacity; this occurs because the rotation of the segments of the flange reduces the longitudinal component of the force carried by them. While this appears to be effective strain softening when considered over the local buckle, it is important to note that at the continuum level, the material continues to harden with increasing plastic strain.

As the applied displacement is cycled, local buckling followed by potential straightening (when the flange is subjected to tension) and subsequent yielding causes cycle-to-cycle degradation (Fig. 2) at the global level. Suzuki and Lignos (2014) as well as Newell and Uang (2008) describe this type of response.

When a sufficient portion of the flange and web lose load-carrying capacity, it is manifested at the global level as a net decrease in moment resulting in a negative slope in the load-deformation curve. This decrease in moment causes curvatures to localize over the buckled zone while the rest of the member unloads elastically. This postpeak response is critical from the standpoint of collapse assessment because the so-called collapse capacity (Ibarra and Krawinkler 2005) is highly sensitive to the negative slope and the localization of curvatures amplifies continuum strains, eventually leading to fracture (Fell et al. 2010).

In cases where the member is not braced adequately, a similar pattern of strength and stiffness degradation may be observed due to lateral torsional buckling (Uang et al. 2015). This paper focuses on laterally braced beam-columns whose softening/degradation response is controlled by local (rather than lateral-torsional) buckling.

Experiments and Continuum Finite-Element Simulation of Cyclically Loaded Beam-Columns

Table 1 summarizes the parameters of physical experiments [conducted previously by Elkady and Lignos (2018a)] as well as CFE simulations conducted as part of this study. These tests and simulations consist of columns with boundary conditions ranging from fixed-fixed to fixed-free, subjected to cyclic lateral displacements under different levels of compressive axial loads. Collectively termed benchmark specimens, they are used to inform aspects of the 2D element formulation (global and local physical response, effective fiber-scale constitutive relationships), as well as to provide results for model validation. Although the physical experiments reflect a "true" response, they represent a limited parameter set; moreover the fiber-level constitutive response (which is an essential input to the nonlocal frame element) cannot be recovered directly from physical tests, in which only the global load-deformation response is monitored. The CFE simulations overcome both these limitations by enabling investigation of additional parameters while also providing access to fiber-level constitutive responses and internal deformations. The CFE models are constructed using the finite-element modeling platform ABAQUS version 6.14 (Hibbitt et al. 2013) using best practices (element types, constitutive response, mesh densities, imperfections) developed by Elkady and Lignos (2015, 2018b) and are able to reproduce various aspects of physical responses with a high degree of accuracy. Kolwankar et al. (2018) provide further discussion of these best practices; the main attributes include four-node shell elements on the order of 25×25 mm, large displacement formulations, and imperfections consistent with manufacturing tolerances to initiate local buckling. The constitutive response of the material is represented through a von Mises yield surface, with combined isotropic-kinematic hardening as per the Voce (1948) and Chaboche et al. (1979) material models to represent low-carbon Grade 50 steel (A992) used in United States construction. Elkady and Lignos (2015, 2018b) provide parameter values for this constitutive model calibrated to cyclic testing of uniaxial coupon specimens. This constitutive response monotonically hardens within each cycle, such that softening-induced mesh dependence is not a problem. Residual stresses were not considered, following observations by Newell and Uang (2008) and Elkady and Lignos (2015) that residual stresses do not significantly affect the response of compact wide-flanged sections since they undergo significant yielding prior to local buckling. Nonetheless, it is noted that these may be significant for slender members prone to lateral torsional buckling (Elkady and Lignos 2018b).

Table 1. Benchmark specimens

Benchmark specimen	Section size	$\frac{b_f}{2t_f}$	$\frac{h}{t_w}$	$\frac{P}{P_y}$ (compressive)	Lateral loading protocol
1[a]	W24 × 146	5.91	33.2	0.2	AISC-symmetric
2[a]	W24 × 146	5.91	33.2	0.5	AISC-symmetric
3[a]	W24 × 146	5.91	33.2	0.2	Collapse consistent
4	W24 × 146	5.91	33.2	0.5	Collapse consistent
5	W24 × 104	8.5	43.1	0.2	AISC-symmetric
6	W24 × 104	8.5	43.1	0.5	AISC-symmetric
7	W24 × 104	8.5	43.1	0.2	Collapse consistent
8	W24 × 104	8.5	43.1	0.5	Collapse consistent

Note: All benchmark specimens are 4,500 mm long.
[a]Indicates both test and simulation are available for this parameter set.

Figs. 3(a–c) compare the experimental response with a complementary CFE simulation (corresponding to Benchmark Specimen 20). Figs. 3(a and b) compare a photograph of post-local-buckling deformations with a rendering of the CFE mesh at the same level of deformation. Fig. 3(c) compares the load-deformation response from the test and CFE simulation. Other quantities (e.g., strain gauge measurements from experiments) are similarly compared to confirm agreement. Once validated in this manner, the CFE models serve as equivalent virtual experiments for the purposes of providing benchmark data for development and validation of the nonlocal models. Referring to Table 1, the varied parameters are the column cross section (to interrogate variation in width–thickness ratios), level of axial load, the moment gradient (indicated by the ratio of peak column moment to shear M/V in Table 1), and the imposed lateral loading protocol. Two types of loading protocols are used, a symmetric loading protocol (Clark et al. 1997) commonly used for component testing and a "collapse-consistent" protocol developed by Suzuki and Lignos (2014, 2015), which simulates highly asymmetric lateral deformation histories characteristic of frame ratcheting prior to earthquake-induced collapse. These parameters are varied in a fractional factorial manner to study the efficacy of the nonlocal formulation under conditions of practical interest. This results in a total of 42 parameter sets (identified in Table 1) that span a wide range of common and realistic design situations. For some of these parameter sets (indicated in the footnote of Table 1), both experiments and CFE simulations are available, whereas only CFE simulations are available for the remaining sets. Subsequent references to benchmark specimens indicate data from the CFE simulations, since results from them are virtually identical to those from the corresponding physical experiment, where it exists. Output from the benchmark specimens retained for nonlocal model development and validation includes load-deformation curves for both lateral and axial deformation,

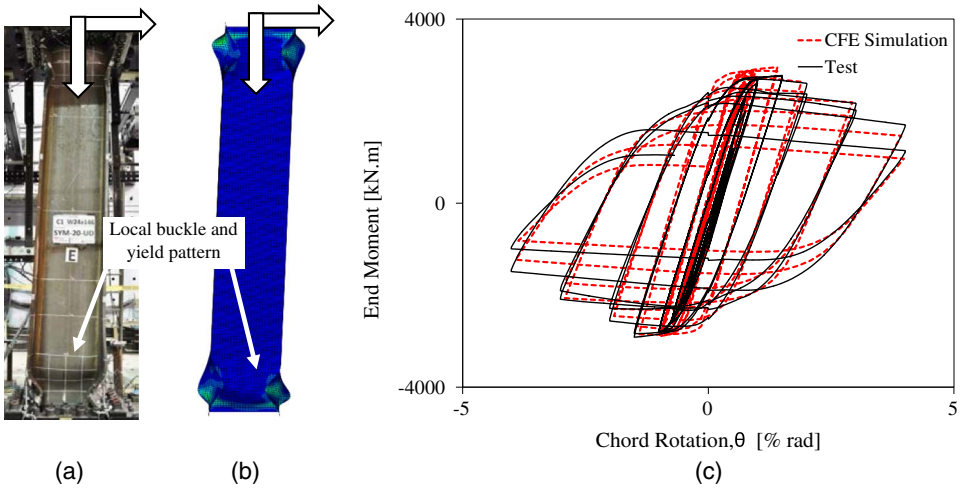

Fig. 3. Representative comparison of results from Benchmark Specimen 1 (W24 × 146, $P/Py = 0.2$) and CFE simulation: (a) test specimen at first cycle with 4% drift; (b) simulation at same loading instant; and (c) load-deformation curve.

continuum strain profiles including local buckle shapes, curvature profiles along the length of a column, the localization length, and fiber-level cyclic stress-strain responses over this localized length.

Determination of curvature profiles from CFE simulations is not straightforward since the plane-sections-remain-plane (PSRP) postulate (which is essential to the definition of curvature) is violated when local buckling occurs. An approach proposed by Kolwankar et al. (2018) is used for this purpose. This approach relies on *effective* longitudinal flange strains, which are the result of material deformation as well as of the projection of buckling-induced flange rotations on the longitudinal axis. Fig. 4(a) schematically illustrates the conceptual definition of these effective strains for one of the benchmark specimens (Specimen 20); Kolwankar et al. (2018) provide mathematical details. These flange strains are subsequently used to estimate curvature. Once the curvature profile is determined for any instant in the loading, the localization length may be inferred from it. Specifically, this corresponds to the region of the member over which curvatures increase (and localize) in the post-peak regime, while the rest of the member shows a net decrease in curvature owing to elastic unloading. For all the benchmark specimens considered in this paper, it is observed that once the peak in the load-deformation curve is reached, the curvatures localize over a length of approximately $L_c = 2.25 \times b_f$; this length remains relatively stable thereafter. This agrees well with prior physical test observations (Suzuki and Lignos 2015; Elkady and Lignos 2018a). Fig. 4(b) shows the obtained constitutive response for the flange (also for Benchmark Specimen 20). The strain is computed as the net displacement normalized over this gauge length, whereas the stress is determined as the longitudinal stress in the element immediately outside the localization zone. Both stress and strain are averaged over the entire flange width. Referring to Fig. 4(b), the stress-strain curve exhibits a classic inelastic buckling response, with the following features: (1) yielding and strain hardening in tension, (2) buckling-induced softening in compression followed by an asymptotic decay toward a residual strength as the amplitude of the local buckle saturates, (3) pinching, i.e., stiffening on reloading in tension as the flange straightens out, and (4) cycle-to-cycle degradation as residual displacements from previous cycles weaken the response. Since the members considered in this paper are all compact (i.e., $b_f/2t_f \leq 65/\sqrt{F_y}$), the local buckling in compression occurs after yielding, with the implication that the peak stress in compression [Fig. 4(b)] is greater than the yield stress.

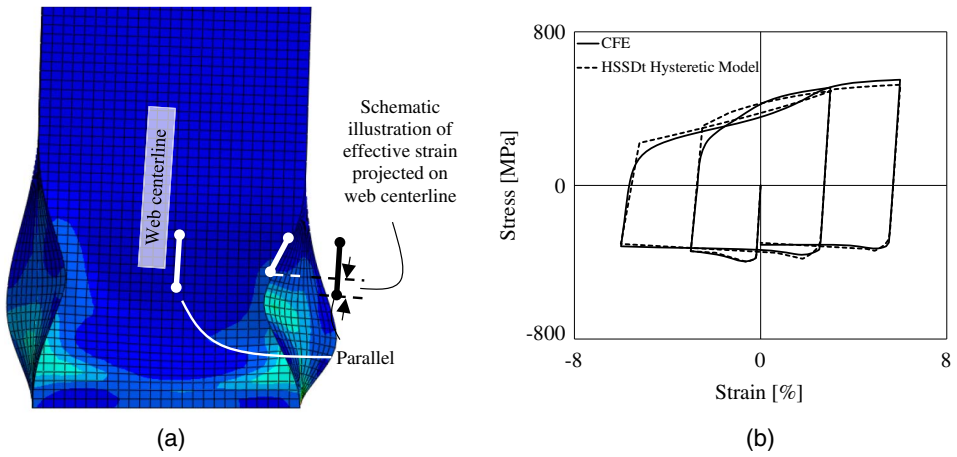

Fig. 4. Effective hysteretic response measured over localized length: (a) CFE showing effective or projected strain; and (b) comparison of effective stress-strain relationship measured over and response as determined by HSSDt model.

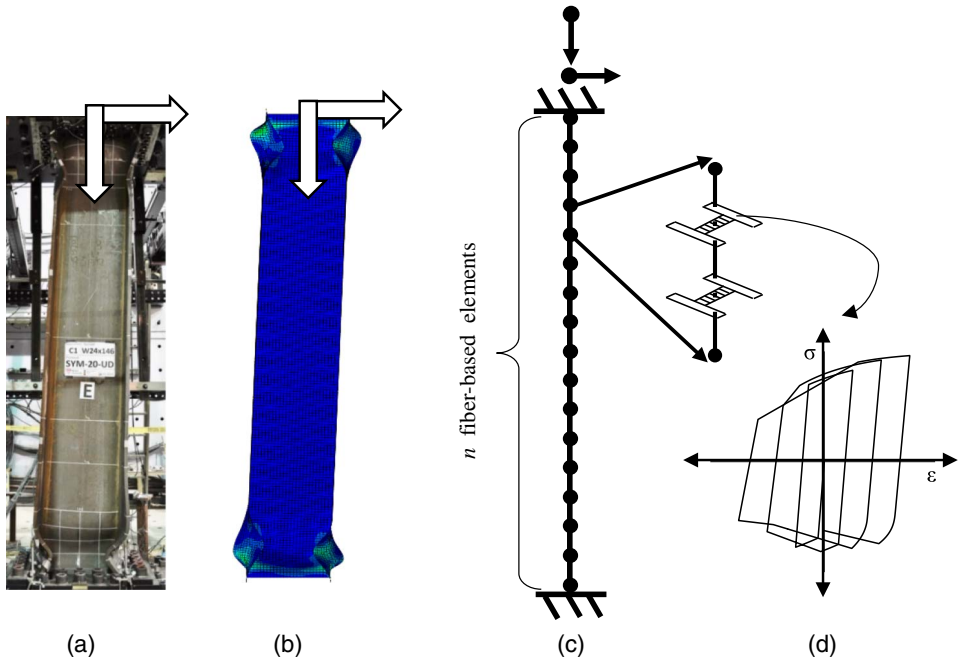

Fig. 5. (a) Test; (b) CFE model; (c) fiber model showing longitudinal and cross-sectional discretization; and (d) HSSDt constitutive model.

A subsequent section discusses the constitutive model [the trace from which is superimposed on the plot in Fig. 4(b)] selected to represent this response, along with recommended practices to calibrate it.

Nonlocal Fiber Models for Cyclically Loaded Beam-Columns

For each benchmark specimen, fiber-based models were constructed in the OpenSees platform (McKenna et al. 2012). Fig. 5 schematically illustrates one such model, alongside a CFE simulation and experiment. The fiber-based models consist of n beam-column elements connected serially, where n may be varied to examine mesh dependence. The elements have the following characteristics:

- They are all planar "displacement-based" frame elements—see McKenna et al. (2012) for Gauss–Lobatto integration.
- The element cross section is discretized into fibers; each flange is a single fiber, whereas the web is discretized into fibers approximately 12.5 mm × web thickness.
- The PSRP assumption is used to calculate strains in any fiber based on the curvature and centerline axial strain.
- Axial forces and moments (i.e., cross-sectional stress resultants) are determined by integrating stresses in individual fibers.
- Element end forces are determined by integrating stress resultants determined at five Gauss points along the length.

Any constitutive model implemented in OpenSees may be assigned to any of the fibers; this includes conventional (local) formulations, which are native to OpenSees, as is the nonlocal formulation presented herein. Implementation of the nonlocal formulation may be subdivided into three main components, discussed in the following subsections. First, a computational framework for the implementation of the formulation must be established; this includes aspects such as finite-element selection, global/structural solution methods, and geometric transformations. Second, a constitutive model to represent cyclic inelastic fiber buckling within this framework must be selected and calibrated. Finally, the nonlocal strain variable must be developed for use with the two preceding components. The development of this variable is contingent on the functional forms of the constitutive model. Consequently, it is presented after the constitutive model.

Computational Framework for Fiber-Based Nonlocal Frame Element

Fig. 6 schematically illustrates the computational framework within which the nonlocal formulation is implemented. The process follows a standard predictor-corrector algorithm (already implemented within OpenSees), which involves computing trial displacement vectors based on the applied loading and a tangent stiffness operator and then minimizing a residual error in the force vector through iteration. Kolwankar et al. (2018) provide a detailed discussion of this process in the context of monotonic loading. The residual error in the force vector is determined with respect to the internal force, which in turn is determined based on element force recovery or state determination (Yang and Leu 1991). As shown in Fig. 6, force recovery is based on the nonlocal formulation. Specifically, the constitutive relationship used to determine internal element forces utilizes the nonlocal, rather than the local, strain variable. This raises challenges in the context of cyclic loading, which are discussed in a subsequent section. Other notable aspects of the computational framework include the following:

- The use of a tangent stiffness matrix that is computed from local strains from the previously converged step, rather than a consistent tangent matrix based on the nonlocal strains (e.g., Jirásek and Patzak 2002) that accelerates convergence.
- The nonlocal formulation considers interaction between locations only in the longitudinal direction, such that interaction between fibers at the same cross section is not considered. Referring to Fig. 5 shown earlier, recall that each flange is represented as a single fiber with constitutive response averaged over the width.

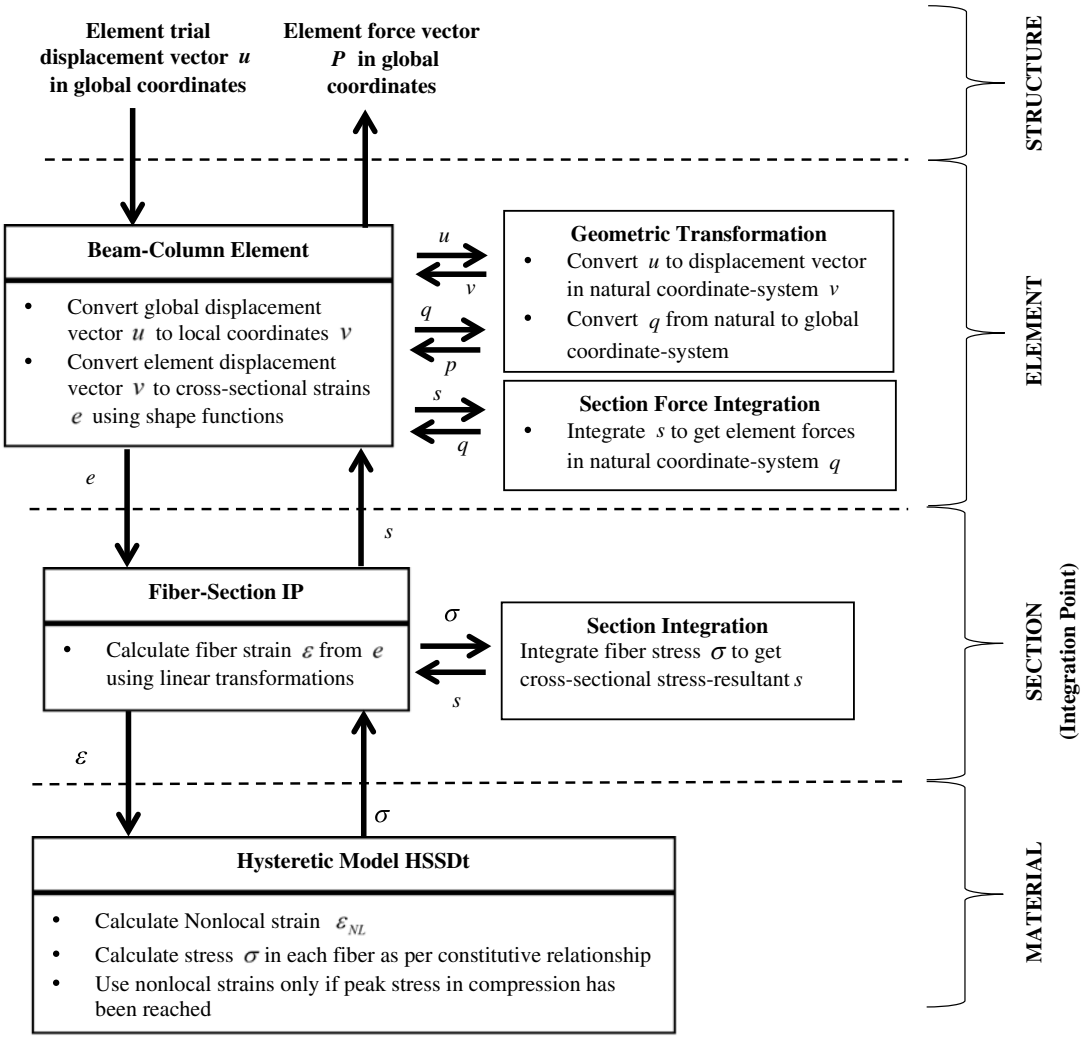

Fig. 6. Algorithmic implementation for displacement-based nonlocal beam-column element with fiber sections.

Constitutive Model for Cyclic Inelastic Buckling of Steel Fibers

A uniaxial cyclic constitutive model (Suzuki and Lignos 2018; Suzuki 2019), henceforth referred to as the SL model, is used to represent inelastic cyclic buckling of steel elements such as flanges and webs. Figs. 7(a and b) illustrate the stress-strain relationship as defined by this model, which was originally developed to simulate local buckling–induced softening in hollow structural steel (HSS) members. The functional form of this model closely follows the fiber-level stress-strain response of flanges in W-sections subject to inelastic buckling. To illustrate this, Fig. 4(b) introduced previously superimposes the trace of the fiber-stress curve (as determined by the SL model) on a counterpart curve obtained from one of the benchmark specimens. Fig. 7(a) illustrates the monotonic backbone of the model in tension and compression, representing the stress-strain relationship corresponding to monotonic loading in either loading direction. Fig. 7(b) illustrates the cyclic evolution of the stress-strain relationship, including key modes of deterioration. Referring to these figures, the main features of the model [detailed in Suzuki and Lignos (2018) and Suzuki (2019)] include the following:

- The monotonic stress-strain curve in compression consists of three parts: the elastic, the postyield, and the postcapping (postpeak) region. The elastic modulus is identical in tension and compression (denoted E), and onset of yielding is defined by the stress σ_y. Combined isotropic/kinematic hardening is defined through four parameters—C, γ, Q, and b. This is a uniaxial interpretation of the Voce (1948) and Chaboche et al. (1979) model by extending the Armstrong and Frederick (1966) multiaxial model that originally included the relaxation term γ. One back stress is considered in this case. Specifically, the parameters C and γ characterize kinematic hardening, whereas the parameters Q and b define isotropic hardening. However, these parameters may be calibrated simultaneously to uniaxial cyclic coupon material testing based on approaches summarized in Smith et al. (2017b) and Sousa and Lignos (2017). A summary of these parameters for mild steels (e.g., A992 Grade 50) is presented in Suzuki and Lignos (2018) and Elkady and Lignos (2018b). Once the capping stress (σ_{y_cap}) is reached, the response softens as defined by two negative moduli E_{d1}, and E_{d2}, which transition at the stress value σ_{d_cap} [Fig. 7(a)].
- The monotonic backbone in tension is similar to that in compression, with the main difference that it hardens monotonically without a capping stress.
- The cyclic response [Fig. 7(b)] is derived from the monotonic response by deteriorating various quantities with respect to the monotonic backbone. On the compression envelope, these

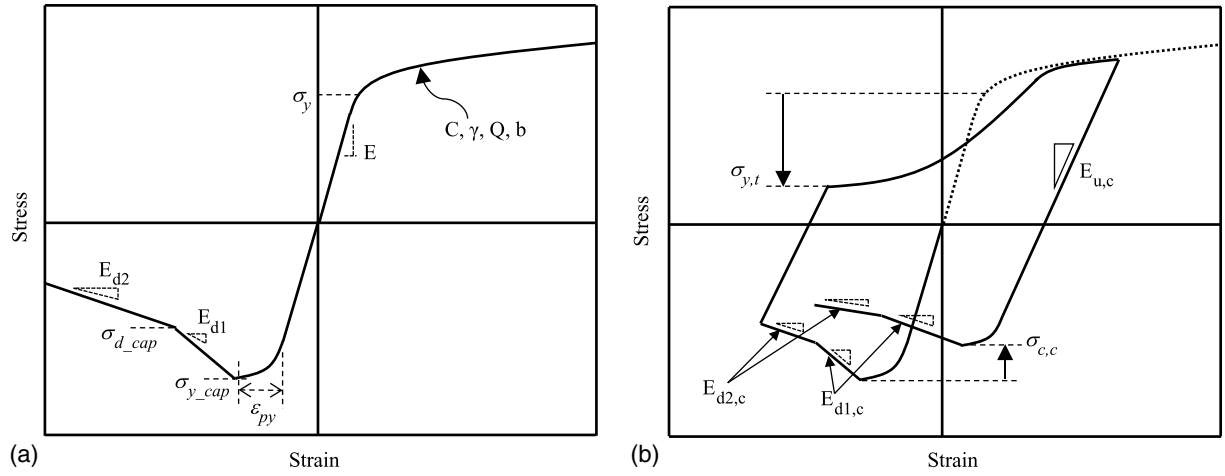

Fig. 7. SL material model: (a) monotonic backbone curve; and (b) degradation in key quantities (strength and postpeak stiffnesses) during cyclic loading.

quantities include the unloading modulus $E_{u,c}$, yield stress σ_y, capping stress $\sigma_{y,c}$, precapping strain $\varepsilon_{py,c}$, and negative moduli $E_{d1,c}$ and $E_{d2,c}$. The deterioration itself depends on cumulative dissipated energy as per a relationship proposed by Rahnama and Krawinkler (1993). The rates of deterioration for each quantity are controlled internally (i.e., hardcoded) within the SL model based on the element slenderness ratio (i.e., $b_f/2t_f$ for the flanges and h/t_w for the webs) as per rules outlined by Suzuki (2019). Utilizing these hardcoded aspects of the SL model [which are further detailed in Suzuki (2019)], nine free parameters (E, σ_y, C, γ, Q, b, σ_{y_cap}, ε_{res}, and σ_{d_cap}) must be estimated to fully describe the uniaxial constitutive model response; this estimation is discussed in a subsequent section.

With respect to the nonlocal formulation presented herein, two aspects of the constitutive model are relevant. From a mathematical standpoint, the constitutive model must be adapted to the nonlocal formulation. From a practical standpoint, it is important to identify parameters that require calibration, along with best practices for conducting this calibration; this is discussed in a following subsection.

Nonlocal Formulation for Inelastic Cyclic Buckling Constitutive Model

As Fig. 6 showed previously, the nonlocal formulation is applied during the force-recovery process to determine element internal forces. This involves operating on strains in the vicinity of the location of interest to determine a nonlocal strain, which is then input to the constitutive relationship discussed earlier. Kolwankar et al. (2018) implemented a nonlocal constitutive formulation within displacement-based beam-column elements. This formulation considered only monotonic loading, with a trilinear backbone curve used to represent softening response. Cyclic effects were neglected. The primary operation of this formulation is to use a nonlocal (or spatially averaged) strain variable as the input into the constitutive model, enabling the insertion of length scale. Eqs. (1)–(4) in what follows summarize the nonlocal strain formulation developed by Kolwankar et al. (2018) for monotonic loading. Specifically, the nonlocal strain ε_{NL} at any "host" location is determined as

$$\varepsilon_{NL} = m \cdot \varepsilon^w + (1-m) \cdot \varepsilon \tag{1}$$

where ε^w is a weighted average of the strain ε in the vicinity of the host location:

$$\varepsilon^w(x) = \int_{L_c} w(x,\xi) \cdot \varepsilon(x,\xi) \cdot d\xi \tag{2}$$

The averaging is conducted via the bell-shaped weighting function $w(x,\xi)$ defined over the length L_c—see Eqs. (3) and (4) in what follows; the term ξ is a local variable:

$$w(x,\xi) = \frac{w'(x,\xi)}{\int_{L_c} w'(x,\xi) \cdot d\xi} \tag{3}$$

and

$$w'(x,\xi) = \frac{15}{8 \cdot L_c}\left(1 - \frac{4 \cdot (x-\xi)^2}{L_c^2}\right) \quad \text{for } |x-\xi| \le L_c/2;$$
$$w'(x,\xi) = 0 \quad \text{for } |x-\xi| > L_c/2 \tag{4}$$

The normalizing term $w'(x,\xi)$ prevents alteration of the homogeneous field. Termed the "over-nonlocal" formulation (Vermeer and Brinkgreve 1994), this combines the strict nonlocal strain (usually determined as ε^w) with the local strain ε through a weighting parameter m. This parameter provides an additional degree of freedom to the localization problem facilitating complete regularization of the localization problem (i.e., regularization with respect to both the load deformation relationship as well as the local strain field). Following Kolwankar et al. (2018), m is selected as 1.5, whereas the characteristic length scale L_c is selected as $2.25 \times b_f$, following the observations from the benchmark specimens discussed earlier.

Extending this formulation to cyclic loading presents special challenges because, as demonstrated by Bazant and Jirasek (2002), the nonlocal strain variable must increase monotonically for convergence. For this reason, many nonlocal formulations for monotonic loading including Bazant and Jirasek (2002) use the plastic, rather than the total, strain since it increases monotonically, unlike the elastic strain, which may decrease owing to unloading. For cyclic loading, neither the elastic nor the plastic strain increases monotonically—this is clearly problematic for convergence. To address this problem, it is recognized that at any instant in loading, one may visualize a "prospective backbone" representing the hypothetical constitutive response that would follow if the cyclic loading were ceased and the material were instead loaded monotonically in either tension or compression.

Following this visualization, the cyclic constitutive model is reinterpreted as a series of monotonic models whose backbones may be updated at each strain reversal based on the degradation

accumulated up to the previous loading cycle. More specifically, at each loading instant, this prospective backbone is based on the degradation rules of the SL model, representing the stress-strain curve the material would follow if only monotonic loading (in either tension or compression) were applied after the most recent zero stress state of the material. For all subsequent loadings at this material point (until the next stress reversal), this may be treated as the effective monotonic response for the purposes of the nonlocal formulation. Such reinterpretation is also convenient within the mathematical structure of the SL model, since at each instant during the loading history the entire prospective backbone in both tension and compression directions (i.e., anticipated stress-strain trajectory assuming no reversals) is predetermined, given the accumulated degradation up to the previous cycle. As an illustration, see Fig. 8(a), which shows three such instants in the loading history, and Figs. 8(b–d), which show the degraded prospective backbone at each of these instants. Referring to these figures, at each instant, the problem is reduced to a monotonic problem, which is tractable within the previously developed formulation of Kolwankar et al. (2018), provided that (1) the degraded backbone is used and (2) the strain quantity for nonlocal averaging, i.e., ε^*, is measured from the most recent intersection of the stress-strain curve with the horizontal axis—see Figs. 8(b–d). The quantity ε^*, represented schematically as the dark arrow along the horizontal axis monotonically increases (notwithstanding sign convention) within each cycle, and thus enables effective application of the nonlocal formulation. With this modification, the cyclic formulation is identical to the monotonic formulation in Eqs. (1)–(4) given earlier, except with the replacement of ε by the in-cycle strain ε^* for each cycle. The offset for the estimation of ε^* is updated each time the backbone curve changes due to degradation. This formulation is implemented within the computational framework illustrated in Fig. 6. Further, it is relevant to note that in the SL model, the offset strain and prospective backbone curve is updated only when the loading direction is reversed and encounters yield in the opposite direction. Thus, during partial unloading-reloading the current backbone curve remains unaffected and ε^* is measured from the same offset. Application of this framework to specific problems (e.g., the benchmark specimens) requires articulation of best practices for model construction as well as parameter calibration. These include the nine free parameters of the uniaxial constitutive model itself (described previously), in addition to the parameters L_c and m of the nonlocal formulation. Based on these parameters, all modes of cyclic deterioration are controlled internally by the SL model based on the $b_f/2t_f$ and h/t_w ratios as per relationships defined by Suzuki (2019). The parameters for the nonlocal formulation are fixed as $L_c = 2.25 \times b_f$ and $m = 1.5$. Once all parameters are thus prescribed, the computational framework, including the nonlocal formulation, is used to simulate both global and local demand parameters (i.e., obtain load-deformation responses and strain distributions) for each of the benchmark specimens. The results of these simulations are discussed in the next section.

Results and Discussion

Each benchmark specimen in Table 1 is simulated using the nonlocal fiber-based element models as shown in Fig. 5, meaning that identical loading protocols, boundary conditions, and axial loads are applied. The nonlocal parameters L_c and m determined as discussed in the previous section. The constitutive parameters corresponding to degradation are tuned to obtain agreement with the benchmark specimens; the other parameters, E, σ_y, C, b, Q, and γ, remain the same because they depend, not on degradation, but material response only. For each fiber-based simulation,

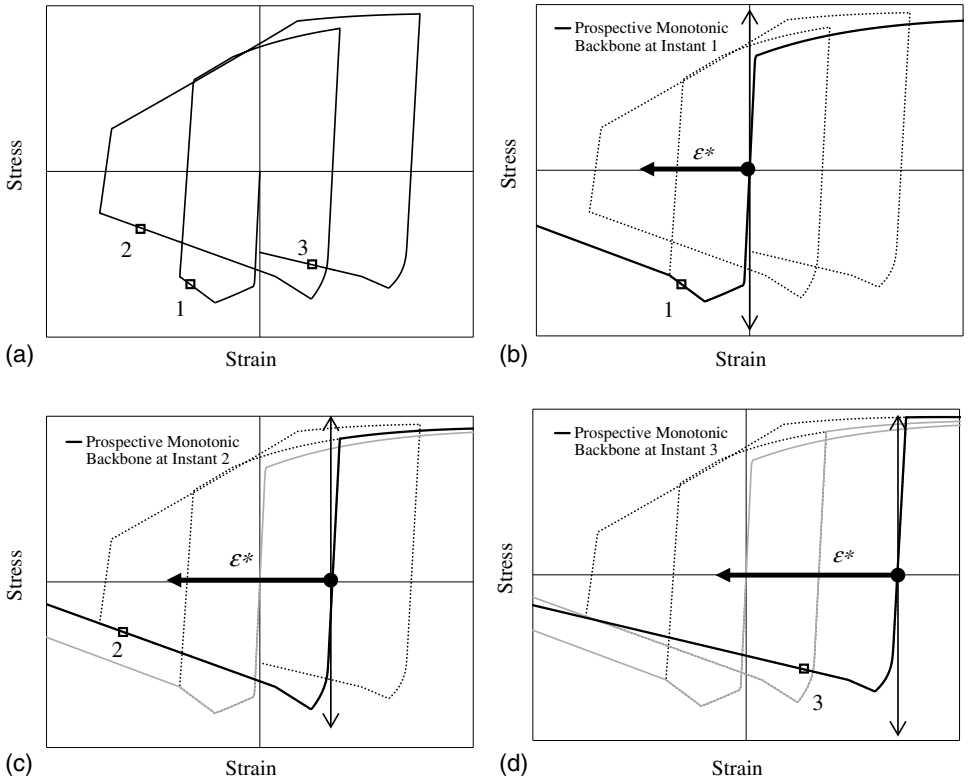

Fig. 8. (a) Hysteretic response using HSSDt model; and (b)–(d) prospective monotonic stress-strain curves at Instants 1, 2, and 3; the method for estimating the in-cycle strain $\varepsilon*$ for each case is shown by the dark arrow.

J. Struct. Eng., 2020, 146(1): 04019174

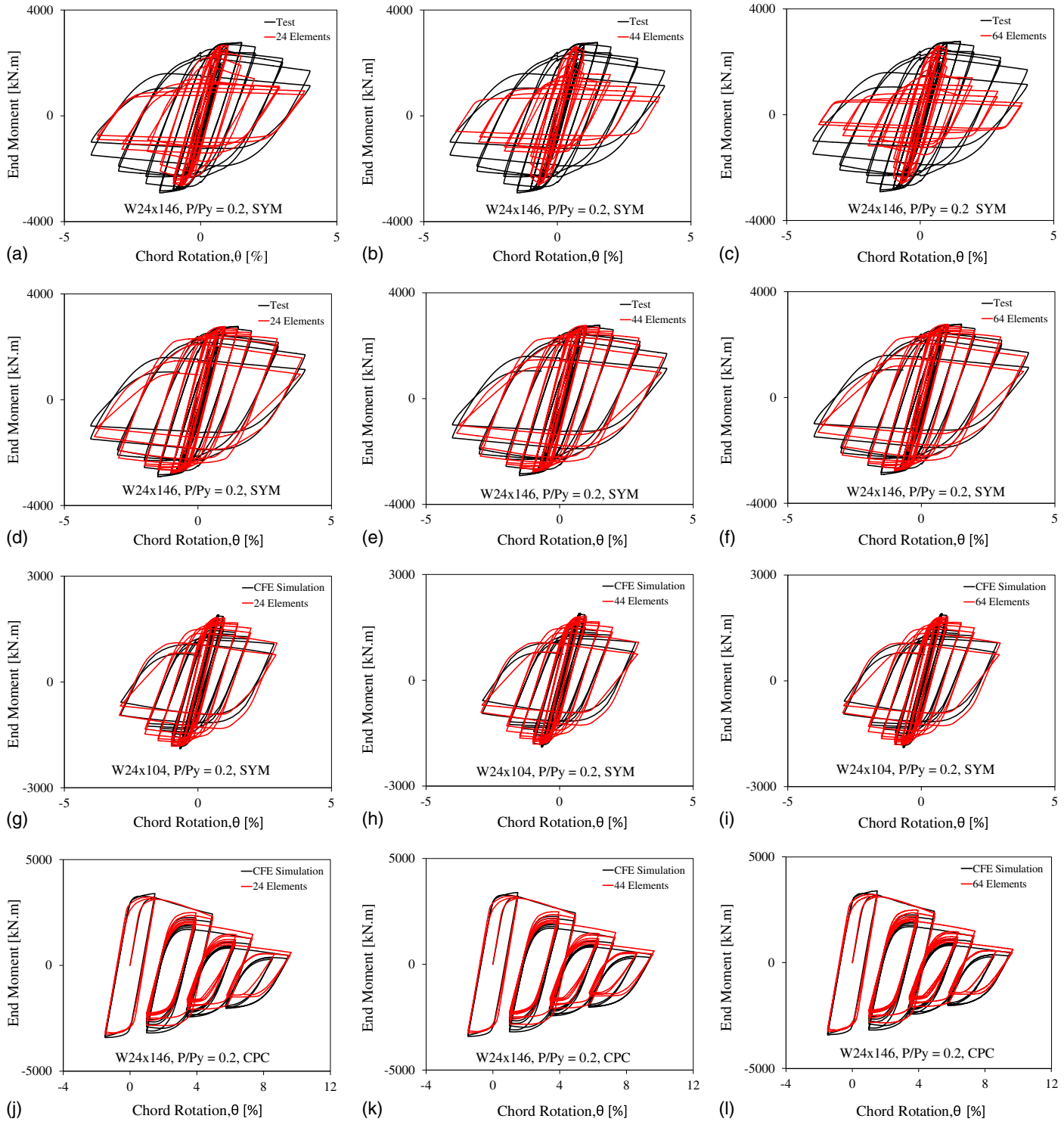

Fig. 9. End moment versus chord rotation curves at axial load of $0.2Py$: (a)–(c) for W24 × 146 with conventional local fiber models; (d)–(f) for W24 × 146 with nonlocal fiber models; (g)–(i) for W24 × 104 with nonlocal fiber models; and (j)–(l) for W24 × 146 with nonlocal fiber models and collapse consistent loading protocol: (a) conventional; (b) conventional; (c) conventional; (d) nonlocal; (e); nonlocal; (f) nonlocal; (g) nonlocal; (h) nonlocal; (i) nonlocal; (j) nonlocal; (k) nonlocal; and (l) nonlocal.

multiple levels of discretization are selected, each with a uniform element size along the length of the column. Additionally, all benchmark specimens are also simulated using conventional local models with identical parameters (except the characteristic length scale and m, which are not included in the local models). Recall that for these benchmark specimens, results from 3D CFE or physical experiments are also available and used as the benchmark representing "true" response. For each simulation (CFE, nonlocal, and local), the following data streams are used for assessment: (1) load-deformation curves, in which the load corresponds to the end moment, and deformation corresponds to the chord rotation of the column (i.e., lateral deformation divided by length);

(2) evolution of peak curvature at the fixed support; and (3) the lateral-versus-axial deformation curves. Studying these disparate data streams provides a rigorous examination of the proposed formulation to simulate important aspects of response. The first (load-deformation response) is important from the standpoint of system-level simulation; the second (curvature profile) is important for assessing downstream damage and fracture limit states; the third is important from the standpoint of residual axial displacements that may control decisions regarding building replacement (Inamasu et al. 2018).

Figs. 9(a–l) show the load-deformation curves of the fiber-based simulations with the conventional (local) and nonlocal models overlaid on counterpart results (as determined from the CFE simulations) from selected benchmark specimens. Figs. 9(a–c) (i.e., the first row of tiles) show results from fiber models with the conventional (local) formulation for one benchmark specimen (Specimen 20) for three different levels of discretization (24, 44, and 64 elements). These figures reconfirm the pathological mesh sensitivity of conventional fiber models in which the length scale is absent, such that models with greater mesh refinement show steeper negative slopes and very rapid flexural strength degradation. The mesh sensitivity is especially severe for cyclic response, as compared to monotonic response (Kolwankar et al. 2018). This may be attributed to two effects: (1) within the current cycle, the response is mesh-sensitive in a manner analogous to monotonic loading, and (2) error accumulation over multiple cycles, since the degraded stress-strain relationship for each cycle is a function of the energy dissipation within previous cycles, which is mesh sensitive in itself. Figs. 9(d–f) illustrate counterpart results (for the same benchmark specimen, i.e., Specimen 20) from the nonlocal fiber models, which also include the length scale. Figs. 9(g–l) illustrate similar results from nonlocal models, albeit for different benchmark specimens [Specimen 32 for Figs. 9(g–i) and Specimen 26 for Figs. 9(j–l)], to demonstrate the efficacy of the method for a different cross section, as well as loading protocol. For these benchmark specimens, the results of conventional fiber models are not shown since they are qualitatively similar (in terms of pathological mesh dependence) to those shown in Figs. 9(a–c). Referring to Figs. 9(a–l), the main observations are as follows: (1) the nonlocal fiber model successfully mitigates mesh sensitivity in load-deformation response across a range of cross-sectional shapes, axial load ratios, and loading histories; and (2) the prescribed methodology for calibration of the model, including the characteristic length, is able to simulate response (in a blind sense) across this range of parameters.

Figs. 10(a and b) show the profile of the curvature in Benchmark Specimen 20 at a drift excursion of 3%; the results are representative of all the benchmark specimens. Of these, Fig. 10(a) shows results from the conventional (local) formulation, whereas Fig. 10(b) shows results from the nonlocal formulation. The observations are similar to those noted for Figs. 9(a–l) and i.e., the conventional fiber approach is highly mesh sensitive [note the wide variation in curvatures for a given x/L in the localized region in Fig. 10(a)], whereas the nonlocal fiber model (along with the calibration process) is able to simulate responses across different configurations in a mesh-independent manner. Fig. 10(c) plots the predicted curvatures at a value of $x/L = 0.02$ (i.e., in the localized zone), also at 3% drift, against the number of elements for both the conventional and the nonlocal formulation. With reference to the figure, the plot for the nonlocal formulation shows convergence, as opposed to the observed divergence for the conventional formulation. Specifically, the percentage error decreases to less than 5% once the element size is refined beyond $L_c/10$. Figs. 11(a and b) show the evolution of axial deformation of the column (Benchmark Specimen 20) as cyclic lateral loading is applied. From a physical

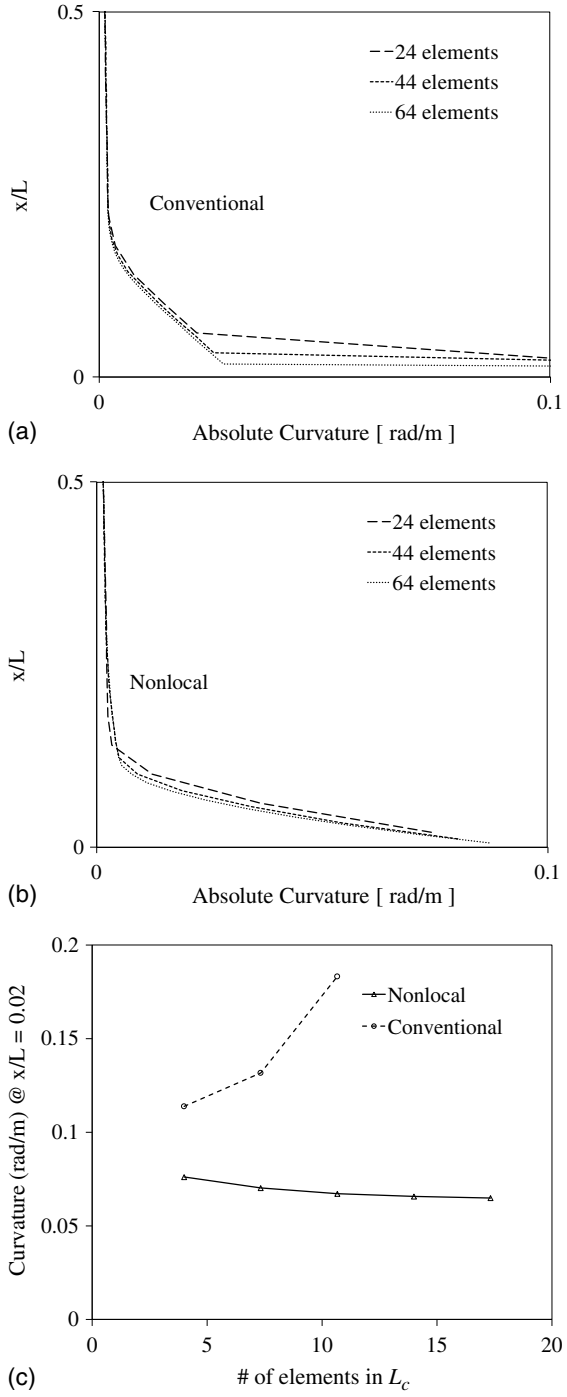

Fig. 10. Curvature profile for W24 × 146 with $P/Py = 0.2$ at peak of 3% drift excursion: (a) with conventional formulation; (b) with nonlocal formulation; and (c) curvature at $x/L = 0.02$ for increasing number of elements.

standpoint, this deformation [which is well documented in literature; see Elkady and Lignos (2015, 2018b) and Chen et al. 2004] arises due to the progressive and irrecoverable "folding" of the flanges and the web due to local buckling, resulting in a net shortening of the column—see prior discussion accompanying Fig. 2. From a practical standpoint, this axial shortening (which is residual in nature) has significant implications for postearthquake repair/retrofit, such that large axial shortening may result in demolition (Suzuki and Lignos 2015, 2018; Inamasu et al. 2018). Consequently, simulation of this effect is of interest for sophisticated

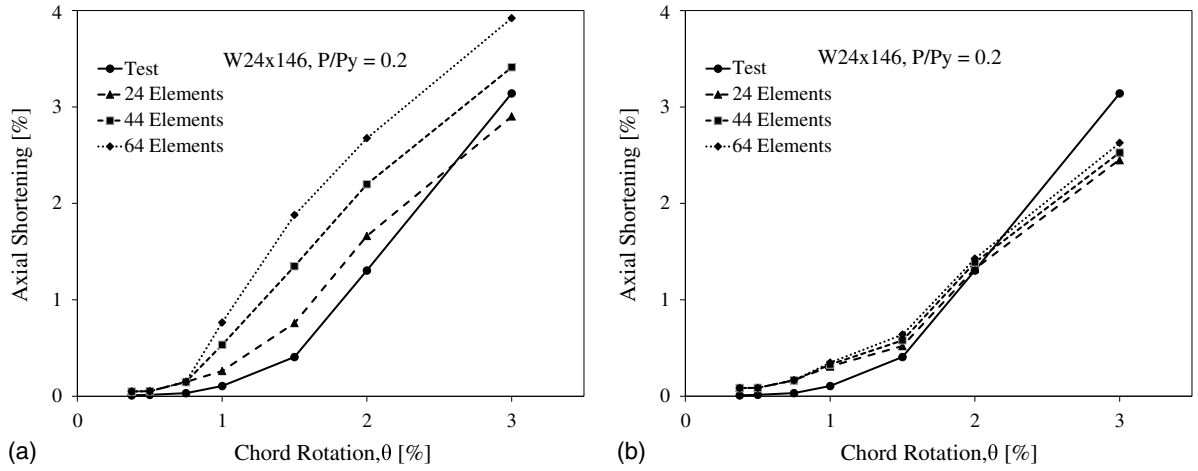

Fig. 11. Axial shortening versus chord rotation for W24 × 146 with $P/Py = 0.2$ at peak of last cycle of each excursion: (a) with conventional local fiber model; and (b) with nonlocal fiber model.

system-level performance assessment. Figs. 11(a and b) provide an examination of the fiber element approach to simulate this response, for both conventional [Fig. 11(a)] and nonlocal [Fig. 11(b)] formulations. In each case, results from multiple discretizations are overlaid on the counterpart CFE curves for Benchmark Specimen 1; results for other specimens are qualitatively similar. Both the local and nonlocal fiber models are able to simulate the axial shortening response; this is in contrast to concentrated hinge models, which usually simulate only flexural response. Note that the simulation of this response is contingent on the specification of softening constitutive response of the web as well as the flanges. However, only the nonlocal fiber models are able to simulate the response with mesh independence (and convergence with mesh refinement). It is important to note that in all instances, the nonlocal approach is able to function effectively only if a sufficient number of elements (or Gauss points) are provided within the characteristic length; element sizes greater than the characteristic length produce meaningless results. For the problems considered in this paper, more than three elements with five Gauss points each over the characteristic length L_c result in an acceptable degree of mesh convergence (error less than 2% upon further refinement).

Suggested Practices for Constitutive Model Parameter Estimation

The foregoing discussion focused on the efficacy of the nonlocal formulation in reproducing response without mesh dependence. To this end (i.e., to minimize confounding effects due to other types of error), the material constitutive parameters were selected to match benchmark specimen response. When the model is applied in a predictive sense, such benchmark response may not be available a priori, requiring parameter estimation. Based on previous studies (Kolwankar et al. 2018) as well as the best-fit parameters estimated in this paper, the following recommendations are suggested for constitutive parameter estimation—these result in relatively good agreement with benchmark specimen data, although not as close as that shown in Figs. 9(a–l).

1. The parameters E, σ_y, C, γ, Q, and b corresponding to elastic response and strain hardening may be calibrated directly from uniaxial cyclic coupon tests (monotonic and cyclic) since they do not pertain to localization as discussed in Suzuki (2019). For this paper, parameter values determined from the test data of Elkady and Lignos (2015, 2018b) were used for typical A992 Grade 50 steel.
2. The capping stress σ_{y_cap} at which local buckling initiates may be determined by the following empirical equation:

$$\sigma_{y\_cap} = 1.1 \times \sigma_u - 2.17 \times (b_f/2t_f) \tag{5}$$

   In the preceding equation [developed by Kolwankar et al. (2018) through regression within the range of $5.92 \le b_f/2t_f \le 8.5$], σ_u is the ultimate stress of the steel material, whereas $b_f/2t_f$ is the flange width-thickness ratio.
3. The negative moduli, $E_{d1,m}$, $E_{d2,m}$, may be determined through the following equations, with reference to Fig. 7:

$$E_{d1,m} = (\sigma_{d\_cap} - \sigma_{y\_cap})/\varepsilon_{res} \tag{6}$$

$$E_{d2,m} = 0.2 * E_{d2,m} \tag{7}$$

4. In the preceding equations, the terms ε_{res} and σ_{d_cap} must be estimated. Equations based on regression against fiber-level data from CFE simulations are developed for this purpose:

$$\sigma_{d\_cap} = \sigma_y - 1.44\frac{b_f}{2t_f} \ge 0 \tag{8}$$

   and

$$\varepsilon_{res} = 0.15 - 0.014\frac{b_f}{2t_f} \ge \frac{\sigma_y}{E} + \frac{\sigma_{cr} - \sigma_y}{h \times E} \tag{9}$$

5. The constitutive parameters for the web may be determined in a similar manner. In fact, the CFE simulations suggest that replacing the term $b_f/2t_f$ by the term h_w/t_w in the preceding equations results in satisfactory agreement with the effective constitutive response of the web as well. Nonetheless, it is reemphasized that the foregoing relationships are provided only as suggested practices based on observations and statistical regressions against a fairly limited data set; they do not materially influence the efficacy of the nonlocal formulation itself.

Summary, Conclusions, and Limitations

Simulation of local buckling–induced softening in frame members is critical for collapse assessment, particularly under seismic

loading. However, challenges are encountered when simulating this response using conventional fiber-based line or frame elements. Specifically, representing local buckling through effective constitutive softening without a regularizing length scale results in a nonelliptic boundary-value problem that manifests as severe mesh dependence when solved numerically. Previous research by the authors addressed this through a nonlocal formulation that introduces a length-scale parameter, thereby regularizing the problem. However, this research was limited to a single fiber (Kolwankar et al. 2017) and to a 2D frame element subjected to monotonic loading (Kolwankar et al. 2018). This article presents the extension of this methodology to a 2D frame element subjected to reversed cyclic loading with inelastic cyclic buckling that is characteristic of seismic loading. The implementation of this methodology in the open-source software OpenSees is presented along with recommended practices for parameter calibration. A comprehensive set of physical tests complemented by CFE simulations are conducted to inform as well as validate the approach. These simulations investigate a range of parameters, including the cross-sectional shape, moment gradient, axial load ratio, and lateral loading history.

The approach includes five main elements: (1) estimation of physical length associated with inelastic cyclic local buckling; (2) representation of fiber-level constitutive response associated with this phenomenon through an appropriate uniaxial constitutive model; (3) a nonlocal formulation that is able to mitigate the singularity that arises from softening response, which is somewhat challenging within the context of cyclic loading; (4) numerical implementation of this formulation in OpenSees; and (5) recommended procedures for calibration and selection of inputs for this implementation. Combining these elements results in a framework that is able to simulate key aspects of response (load-deformation, curvature distribution) in a mesh-independent manner, across a range of parameters and loadings. The framework retains the attractive features of fiber-based modeling, including explicit simulation of P-M interactions, simulation of the initiation and spread of plasticity in arbitrary locations, and the ability to generalize cross-sectional responses from fiber- or material-level calibrations.

The efficacy of the framework is examined against results from CFE simulations. The CFE simulations (which were previously validated against test data) are able to directly simulate the processes of inelastic cyclic local buckling and serve as a rigorous testbed for assessing the proposed framework. Various response quantities are compared between the CFE and the nonlocal fiber-based models; these include the load-deformation response, evolution of localized deformation (curvature), and member axial shortening, each of which is important from a performance assessment viewpoint. The main finding is that the nonlocal fiber models (with appropriate calibration and input selection, as recommended herein) successfully reproduce all these aspects of response, without mesh sensitivity. On the other hand, the conventional (local) fiber-based models suffer from severe mesh sensitivity, such that their postpeak response is difficult to interpret for performance and collapse assessment. Moreover, unlike the conventional models, the nonlocal fiber models also return objective estimates of local deformation (e.g., curvature), which may be used in conjunction with damage mechanics models (e.g., Smith et al. 2017a) for the assessment of fracture or other types of damage. In summary, the nonlocal fiber model provides an attractive approach to simulating steel moment-resisting frame systems subject to seismic or other types of collapse by retaining favorable aspects of conventional fiber modeling while overcoming some of its main limitations. In terms of analysis time, the nonlocal formulation requires roughly 1/50 of the time of the CFE models (for the considered benchmark specimens). On the other hand, it is roughly five times slower than conventional fiber models. Nonetheless, considering the overall context, the performance of the nonlocal framework may be considered attractive because (1) the nonlocal formulation provides accuracy and mesh independence similar to CFE with a 50–100 times increase in speed and (2) the slowdown with respect to conventional fiber models (with pathological mesh dependence) is relatively modest such that analyses of entire frames may be conveniently carried out on a desktop computer within minutes.

In closing, it is important to note that the framework has several limitations. These represent areas of caution in its application, as well as areas for refinement and future research. First, the presented approach addresses only 2D frame elements focusing on only one response mode (inelastic cyclic local buckling), thereby disregarding 3D modes of response (such as lateral torsional buckling or biaxial bending) that often control response, especially under cyclic loading (Elkady and Lignos 2018a, b; Uang et al. 2015). The approach inherits assumptions of the fiber modeling approach, such as the PSRP assumption, which is questionable, especially under large-amplitude local buckling. A consequence of this is that curvatures from CFE simulations cannot be defined rigorously; therefore, the curvatures obtained from the nonlocal fiber models (albeit objective) may be interpreted only in a relative sense between different simulations. The guidelines for calibration and input selection are informed only for a limited number of parameters and for I-shaped rolled steel sections, such that extrapolation beyond these parameters must be carried out with caution. Another limitation is that the proposed formulation does not explicitly consider the effect of residual stresses, with the assumption that their influence is modest under reversed cyclic loading. However, significant residual stresses may be present in some cases (e.g., in welded members), and these may affect local buckling patterns and associated response. This is outside the scope of the current formulation. These limitations may be overcome in future research. Nonetheless, the approach has numerous appealing features (mesh objectivity, spread of plasticity, P-M interaction, generalizability) when situated within the current spectrum of simulation tools, ranging from the computationally facile phenomenological hinge models to the more intensive CFE simulations. As such, the approach provides a way to balance sophistication and accuracy with computational expense when simulating steel frames subject to seismic excitation.

Acknowledgments

This work was supported by the National Science Foundation (Grant No. CMMI 1434300), as well as graduate fellowships from the University of California at Davis. The findings and opinions presented in this paper are entirely those of the authors.

References

AISC. 2016. *Seismic provisions for structural steel buildings*. AISC 341. Chicago: AISC.

Armstrong, P. J., and C. O. Frederick. 1966. *A mathematical represenation of the multiaxial Bauschinger effect*. Berkeley, UK: Berkeley Nuclear Laboratories, Research and Development Dept.

ASCE. 2017. *Minimum design loads for buildings and other structures*. ASCE/SEI-7. Reston, VA: ASCE.

Bazant, Z. P., and M. Jirasek. 2002. "Nonlocal integral formulations of plasticity and damage: Survey of progress." *J. Eng. Mech.* 128 (11): 1119–1149. https://doi.org/10.1061/(ASCE)0733-9399(2002)128:11(1119).

Chaboche, K. D. V., V. Dang, and G. Codier. 1979. "Modelization of the strain moment effect on the cyclic hardening of 316 stainless steel." In *Proc., Structural Mechanics in Reactor Technology—SmiRT 5*, L11. Raleigh, NC: International Association for Structural Mechanics in Reactor Technology.

Chen, C.-H., W.-C. Lai, P. Cordova, G. G. Deierlein, and K. C. Tsai. 2004. "Pseudo-dynamic testing of a full-scale RCS frame: Part 1—Design, construction, and testing." In *Proc., 13th World Conf. on Earthquake Engineering*. Vancouver, BC: International Association for Earthquake Engineering.

Clark, P., K. Frank, H. Krawinkler, and R. Shaw. 1997. *Protocol for fabrication, inspection, testing, and documentation of beam-column connection tests and other experimental specimens*. Rep. No. SAC/BD-97/02. Washington, DC: FEMA.

Coleman, J., and E. Spacone. 2001. "Localization issues in force based frame elements." *J. Struct. Eng.* 127 (11): 1257–1265. https://doi.org/10.1061/(ASCE)0733-9445(2001)127:11(1257).

Dides, M. A., and J. C. de la Llera. 2005. "A comparative study of concentrated plasticity models in dynamic analysis of building structures." *Earthquake Eng. Struct. Dyn.* 34 (8): 1005–1026. https://doi.org/10.1002/eqe.468.

Elkady, A., and D. G. Lignos. 2015. "Analytical investigation of the cyclic behavior and plastic hinge formation in deep wide-flange steel beam-columns." *Bull. Earthquake Eng.* 13 (4): 1097–1118. https://doi.org/10.1007/s10518-014-9640-y.

Elkady, A., and D. G. Lignos. 2018a. "Full-scale testing of deep wide-flange steel columns under multiaxis cyclic loading: Loading sequence, boundary effects, and lateral stability bracing force demands." *J. Struct. Eng.* 144 (2): 04017189. https://doi.org/10.1061/(ASCE)ST.1943-541X.0001937.

Elkady, A., and D. G. Lignos. 2018b. "Improved seismic design and nonlinear modeling recommendations for wide-flange steel columns." *J. Struct. Eng.* 144 (9): 04018162. https://doi.org/10.1061/(ASCE)ST.1943-541X.0002166.

Fell, B. V., A. M. Kanvinde, and G. G. Deierlein. 2010. *Large-scale testing and simulation of earthquake induced ultra low cycle fatigue in bracing members subjected to cyclic inelastic buckling*. Technical Rep. No. 172. Stanford, CA: Stanford Univ.

FEMA. 2009. *Quantification of building seismic performance factors*. FEMA-P695. Washington, DC: FEMA.

Hibbitt, D., B. Karlsson, and P. Sorensen. 2013. *Abaqus/CAE user's guide, ABAQUS 6.11*. Providence, RI: Dassault Systèmes Simulia.

Ibarra, L. F., and H. Krawinkler. 2005. *Global collapse of frame structures under seismic excitations*. Technical Rep. No 152. Stanford, CA: Stanford Univ.

Ibarra, L. G., R. Medina, and H. Krawinkler. 2005. "Hysteretic models that incorporate strength and stiffness deterioration." *Earthquake Eng. Struct. Dyn.* 34 (12): 1489–1511. https://doi.org/10.1002/eqe.495.

Inamasu, H., D. Lignos, and A. M. Kanvinde. 2018. "Effect of column base flexibility on earthquake induced residual deformation of steel columns." In *Proc., 9th Int. Conf. on the Behavior of Steel Structures in Seismic Areas STESSA 2018*. Christchurch, New Zealand: Steel Construction New Zealand Incorporated.

Jirásek, M., and B. Patzak. 2002. "Consistent tangent stiffness for nonlocal damage models." *Comput. Struct.* 80 (14–15): 1279–1293. https://doi.org/10.1016/S0045-7949(02)00078-0.

Kasai, K., T. Nam, and B. Maison. 2016. "Structural collapse correlative analysis using phenomenological fiber hinge elements to simulate two-directional column deteriorations." *Earthquake Eng. Struct. Dyn.* 45 (10): 1581–1601. https://doi.org/10.1002/eqe.2742.

Khaloo, A. R., and S. Tariverdilo. 2002. "Localization analysis of reinforced concrete members and softening behavior." *J. Struct. Eng.* 128 (9): 1148–1157. https://doi.org/10.1061/(ASCE)0733-9445(2002)128:9(1148).

Khaloo, A. R., and S. Tariverdilo. 2003. "Localization analysis in softening RC frame structures." *Earthquake Eng. Struct. Dyn.* 32 (2): 207–227. https://doi.org/10.1002/eqe.220.

Kolwankar, S. S., A. M. Kanvinde, M. Kenawy, and S. Kunnath. 2017. "A uniaxial nonlocal formulation for geometric nonlinearity induced necking and buckling localization in a steel bar." *J. Struct. Eng.* 143 (9): 04017091. https://doi.org/10.1061/(ASCE)ST.1943-541X.0001827.

Kolwankar, S. S., A. M. Kanvinde, M. Kenawy, D. G. Lignos, and S. Kunnath. 2018. "Simulating local buckling-induced softening in steel members using an equivalent nonlocal material model in displacement-based fiber elements." *J. Struct. Eng.* 144 (10): 04018192. https://doi.org/10.1061/(ASCE)ST.1943-541X.0002189.

LATBSDC (Los Angeles Tall Building Structural Design Council). 2017. "An alternative procedure for seismic analysis and design of tall buildings located in the Los Angeles region, 2017 edition." Accessed March 20, 2018. http://www.tallbuildings.org/.

Lignos, D. G., T. Hikino, Y. Matsuoka, and M. Nakashima. 2013. "Collapse assessment of steel moment frames based on e-defense full-scale shake table collapse tests." *J. Struct. Eng.* 139 (1): 120–132. https://doi.org/10.1061/(ASCE)ST.1943-541X.0000608.

Lignos, D. G., and H. Krawinkler. 2013. "Development and utilization of structural component databases for performance-based earthquake engineering." *J. Struct. Eng.* 139 (8): 1382–1394. https://doi.org/10.1061/(ASCE)ST.1943-541X.0000646.

Lignos, D. G., H. Krawinkler, and A. Whittaker. 2011. "Prediction and validation of sidesway collapse of two scale models of a 4-story steel moment frame." *Earthquake Eng. Struct. Dyn.* 40 (7): 807–825. https://doi.org/10.1002/eqe.1061.

McKenna, F., G. L. Fenves, M. H. Scott, and B. Jeremic. 2012. *Open system for earthquake engineering simulation (OpenSees)*. Berkeley, CA: Pacific Earthquake Engineering Research Center, Univ. of California.

Newell, J. D., and C. M. Uang. 2008. "Cyclic behavior of steel wide-flange columns subjected to large drift." *J. Struct. Eng.* 134 (8): 1334–1342. https://doi.org/10.1061/(ASCE)0733-9445(2008)134:8(1334).

PEER (Pacific Earthquake Engineering Research Center). 2010. *Guidelines for the performance-based seismic design of tall buildings*. PEER Rep. No. 2010/05. Berkeley, CA: PEER.

Rahnama, M., and H. Krawinkler. 1993. *Effects of soft soil and hysteresis model on seismic demands*. Rep. No. 108. Stanford, CA: John A. Blume Earthquake Engineering Center, Stanford Univ.

Salehi, M., and P. Sideris. 2017. "Refined gradient inelastic flexibility-based formulation for members subjected to arbitrary loading." *J. Eng. Mech.* 143 (9): 04017090. https://doi.org/10.1061/(ASCE)EM.1943-7889.0001288.

Salehi, M., and P. Sideris. 2018. "A finite-strain gradient-inelastic beam theory and a corresponding force-based frame element formulation." *Int. J. Numer. Methods Eng.* 116 (6): 380–411. https://doi.org/10.1002/nme.5929.

Sideris, P., and M. Salehi. 2016. "A gradient inelastic flexibility-based frame element simulation." *J. Eng. Mech.* 142 (7): 04016039. https://doi.org/10.1061/(ASCE)EM.1943-7889.0001083.

Smith, C. M., A. Kanvinde, and G. G. Deierlein. 2017b. "Calibration of continuum cyclic constitutive models for structural steel using particle swarm optimization." *J. Eng. Mech.* 143 (5): 04017012. https://doi.org/10.1061/(ASCE)EM.1943-7889.0001214.

Smith, C. M., A. M. Kanvinde, and G. G. Deierlein. 2017a. "A local criterion for ductile fracture under low-triaxiality axisymmetric stress states." *Eng. Fract. Mech.* 169 (Jan): 321–335. https://doi.org/10.1016/j.engfracmech.2016.10.011.

Sousa, A. C., and D. G. Lignos. 2017. *On the inverse problem of classic nonlinear plasticity models—An application to cyclically loaded structural steels*. Technical Rep. No. 231968. Lausanne, Switzerland: Resilient Steel Structures Laboratory, École Polytechnique Fédérale de Lausanne.

Spacone, E., and F. C. Filippou. 1996. "Fibre-beam column model for non-linear analysis of R/C frames: Part I—Formulation." *Earthquake Eng. Struct. Dyn.* 25 (7): 711–725. https://doi.org/10.1002/(SICI)1096-9845(199607)25:7<711::AID-EQE576>3.0.CO;2-9.

Suzuki, Y. 2019. "Earthquake-induced collapse of steel moment resisting frames with conventional and high performance steel columns." Ph.D. dissertation, Dept. of Civil Engineering, McGill Univ.

Suzuki, Y., and D. G. Lignos. 2014. "Development of loading protocols for experimental testing of steel columns subjected to combined high axial

load and lateral drift demands near collapse." In *Proc., 10th National Conf. on Earthquake Engineering*. Anchorage, AK: Earthquake Engineering Research Institute.

Suzuki, Y., and D. G. Lignos. 2015. "Large scale collapse experiments of wide-flange steel beam-columns." In *Proc., 8th Int. Conf. on Behavior of Steel Structures in Seismic Areas (STESSA)*. Shanghai, China: Tongji Univ.

Suzuki, Y., and D. G. Lignos. 2018. "Fiber-based model for earthquake induced collapse simulation of steel frame buildings." In *Proc., 11th US National Conf. on Earthquake Engineering*. Oakland, CA: Earthquake Engineering Research Institute.

Uang, C.-M., G. Ozkula, and J. Harris. 2015. "Observations from cyclic tests on deep slender wide-flange steel beam-column members." In *Proc., Structural Stability Research Council*. Chicago, IL: Structural Stability Research Council.

Valipour, H., and S. Foster. 2009. "Nonlocal damage formulation for a flexibility based frame element." *J. Struct. Eng.* 135 (10): 1213–1221. https://doi.org/10.1061/(ASCE)ST.1943-541X.0000054.

Vermeer, P. A., and R. B. J. Brinkgreve. 1994. "A new effective non-local strain measure for softening plasticity." In *Proc., Localization and Bifurcation Theory for Soil and Rocks*, 89–100. Rotterdam, Nethrelands: A.A. Balkema.

Voce, E. 1948. "The relationship between stress and strain for homogenous deformation." *J. Inst. Met.* 74: 537–562.

Wu, S., and X. Wang. 2008. "Comparison of boundary conditions of gradient elasticity and gradient plasticity." In *Proc., Inaugural Int. Conf. of the Engineering Mechanics Institute*. Minneapolis, MN: Univ. of Minnesota.

Wu, S., and X. Wang. 2010. "Mesh dependence and nonlocal regularization of one-dimensional strain softening plasticity." *J. Eng. Mech.* 136 (11): 1354–1365. https://doi.org/10.1061/(ASCE)EM.1943-7889.0000184.

Yang, Y.-B., and L.-J. Leu. 1991. "Force recovery procedures in nonlinear analysis." *Comput. Struct.* 41 (6): 1255–1261. https://doi.org/10.1016/0045-7949(91)90262-K.

Zhang, G., and K. Khandelwal. 2016. "Modeling of nonlocal damage-plasticity in beams using isogeometric analysis." *Comput. Struct.* 165 (Mar): 76–95. https://doi.org/10.1016/j.compstruc.2015.12.006.